

Improving the $^{30}\text{P}(p,\gamma)^{31}\text{S}$ rate in oxygen-neon novae: Constraints on J^π values for proton-threshold states in ^{31}S

A. Parikh,^{1,2,3,4,*} K. Wimmer,^{3,4,5} T. Faestermann,^{3,4} R. Hertenberg,^{4,6} J. José,^{1,2} R. Longland,¹ H.-F. Wirth,^{4,6} V. Bildstein,^{3,4} S. Bishop,^{3,4} A. A. Chen,^{7,8} J. A. Clark,⁹ C. M. Deibel,^{9,10} C. Herlitzius,^{3,4} R. Krücken,^{3,4,†} D. Seiler,^{3,4} K. Straub,^{3,4} and C. Wrede¹¹

¹Departament de Física i Enginyeria Nuclear, Universitat Politècnica de Catalunya, E-08036 Barcelona, Spain

²Institut d'Estudis Espacials de Catalunya, E-08034 Barcelona, Spain

³Physik Department E12, Technische Universität München, D-85748 Garching, Germany

⁴Maier-Leibnitz-Laboratorium der Münchner Universitäten (MLL), D-85748 Garching, Germany

⁵National Superconducting Cyclotron Laboratory, Michigan State University, East Lansing, Michigan 48824, USA

⁶Fakultät für Physik, Ludwig-Maximilians-Universität München, D-85748 Garching, Germany

⁷Department of Physics and Astronomy, McMaster University, Hamilton, Ontario L8S 4M1, Canada

⁸Excellence Cluster Universe, Technische Universität München, D-85748 Garching, Germany

⁹Physics Division, Argonne National Laboratory, Argonne, Illinois 60439, USA

¹⁰Joint Institute for Nuclear Astrophysics, Michigan State University, East Lansing, Michigan 48824, USA

¹¹Department of Physics, University of Washington, Seattle, Washington 98195, USA

(Received 7 February 2011; published 27 April 2011)

Calculation of the thermonuclear $^{30}\text{P}(p,\gamma)^{31}\text{S}$ rate in oxygen-neon nova explosions depends critically upon nuclear structure information for states within ~ 600 keV of the $^{30}\text{P} + p$ threshold in ^{31}S . We have studied the $^{31}\text{P}(^3\text{He},t)^{31}\text{S}$ reaction at 25 MeV using a high-resolution quadrupole-dipole-dipole-dipole magnetic spectrograph. Tritons corresponding to the states $E_x(^{31}\text{S}) \sim 6.1\text{--}7.1$ MeV were observed at ten angles between $\theta_{\text{lab}} = 10^\circ$ and 55° . States that were only tentatively identified in past studies have been observed unambiguously. For the first time, we have measured and analyzed angular distributions of the $^{31}\text{P}(^3\text{He},t)^{31}\text{S}$ reaction. We present, also for the first time, a consistent set of experimental spin constraints for all except one of the critical proton-threshold states in ^{31}S . Hydrodynamic nova simulations have been calculated in order to assess the impact on nova nucleosynthesis of remaining uncertainties in J^π values of ^{31}S states and the unknown relevant proton spectroscopic factors. We find that these uncertainties may lead to a factor of up to 20 variation in the $^{30}\text{P}(p,\gamma)^{31}\text{S}$ rate over typical nova peak temperatures, which may then lead to a factor of up to 4 variation in the nova yields of Si-Ar isotopes.

DOI: [10.1103/PhysRevC.83.045806](https://doi.org/10.1103/PhysRevC.83.045806)

PACS number(s): 26.30.-k, 25.55.Kr, 27.30.+t, 97.30.Qt

I. INTRODUCTION

Most of the thermonuclear reaction rates thought to be involved in classical nova explosions are constrained by experimental measurements [1,2]. This situation allows for rather precise statements to be made about which nuclear physics measurements are still necessary to improve the input to nova models, so as to better facilitate the quantitative comparison of observations to model predictions. Sensitivity studies that examine the specific impact of current experimental uncertainties in different reaction rates on nova nucleosynthesis predictions are particularly useful in guiding experimental work. For nucleosynthesis in oxygen-neon (ONe) nova explosions, three reactions have been expressly noted with rate uncertainties that have the most significant impact on model predictions: the $^{18}\text{F}(p,\alpha)^{15}\text{O}$, $^{25}\text{Al}(p,\gamma)^{26}\text{Si}$, and $^{30}\text{P}(p,\gamma)^{31}\text{S}$ reactions [3,4].

The $^{30}\text{P}(p,\gamma)^{31}\text{S}$ reaction drives the nuclear activity in ONe novae toward the heaviest species that can be produced in these phenomena (up to $\approx\text{Ca}$, in agreement with spectroscopic observations of nova ejecta), and its rate therefore affects

abundance predictions for these nuclei. In the postprocessing sensitivity study of Iliadis *et al.* (2002) [5], variations in their adopted $^{30}\text{P}(p,\gamma)^{31}\text{S}$ rate (derived from statistical model calculations) by a factor of 100 modified nova model abundance predictions of multiple isotopes within $A = 30\text{--}38$ by at least a factor of 2 (relative to calculations with their standard rate). Similarly, in the study of José *et al.* (2001) [6], reduction of their $^{30}\text{P}(p,\gamma)^{31}\text{S}$ rate (also based upon statistical model calculations) by a factor of 100 within a self-consistent one-dimensional (1D) hydrodynamic model dramatically changed abundances within $A = 30\text{--}38$ by factors of 2–10. Such effects have consequences not only for the interpretation of observations of nova ejecta, but also for the possible nova paternity of presolar grains. Such grains are identified through the measurement of isotopic ratios with values characteristic of nova nucleosynthesis. Of particular relevance here is the large (relative to solar) $^{30}\text{Si}/^{28}\text{Si}$ ratio expected for grains originating from environments surrounding ONe novae [7]. This ratio is sensitive to the competition between the rate of ^{30}P β^+ decay ($t_{1/2} = 2.5$ min, to ^{30}Si) and that of the $^{30}\text{P}(p,\gamma)^{31}\text{S}$ reaction.

Direct measurement of the $^{30}\text{P}(p,\gamma)^{31}\text{S}$ reaction [$Q = 6130.9(4)$ keV [8,9]] at energies relevant for ONe nova explosions ($T_{\text{peak}} = 0.2\text{--}0.4$ GK) is not yet possible due to the lack of sufficiently intense radioactive ^{30}P beams.

* anuj.r.parikh@upc.edu

† Present address: TRIUMF, Vancouver, BC, V6T 2A3, Canada.

Indirect methods must therefore be exploited: nuclear structure information is required for states within ~ 600 keV of the $^{30}\text{P} + p$ threshold in ^{31}S . Under the assumption of narrow, isolated resonances, the resonant rate $\langle\sigma v\rangle$ of the $^{30}\text{P}(p,\gamma)^{31}\text{S}$ reaction can be calculated (in $\text{cm}^3 \text{s}^{-1} \text{mol}^{-1}$) as [10]

$$N_A \langle\sigma v\rangle = 1.5399 \times 10^{11} (\mu T_9)^{-3/2} \sum_i (\omega\gamma)_i \times \exp(-11.605 E_{R,i}/T_9), \quad (1)$$

where N_A is the Avogadro constant, T_9 is the temperature in GK, μ is the reduced mass of the $^{30}\text{P} + p$ system in u , and the $E_{R,i}$ are resonance energies in MeV. The resonance strength $(\omega\gamma)$ [in MeV in Eq. (1)] can be expressed as

$$(\omega\gamma) = \frac{2J_R + 1}{(2J_p + 1)(2J_t + 1)} \frac{\Gamma_p \Gamma_\gamma}{\Gamma}, \quad (2)$$

where J_R , J_p ($=1/2$), and J_t ($=1$) are the spins of the resonance in ^{31}S , the proton, and ^{30}P (ground state), respectively. The total width of a resonance Γ is the sum of the proton and γ -ray partial widths (Γ_p and Γ_γ , respectively) for ^{31}S states relevant to nucleosynthesis in ONe novae. The sum in Eq. (1) allows for the contributions of all resonant states through which the reaction may proceed at the temperature of interest.

There has been significant recent activity concentrated on determining the structure of ^{31}S above the $^{30}\text{P} + p$ threshold precisely [11–17]; a number of states have been identified and some spin-parity assignments have been made. No experimental information is available on (p,γ) resonance strengths (or partial widths) for states below $E_x(^{31}\text{S}) = 6.7$ MeV. Thermonuclear $^{30}\text{P}(p,\gamma)^{31}\text{S}$ rates over nova temperatures have been calculated in the past [13–16] using tentative ^{31}P , ^{31}S mirror assignments, shell-model calculations, and/or educated guesses to estimate the unknown partial widths. For example, the proton partial width Γ_p in Eq. (2) can be estimated via [10]

$$\Gamma_p = \frac{2\hbar^2}{\mu a^2} P_l C^2 S_l \theta_{\text{sp},l}^2, \quad (3)$$

where μ is the reduced mass of the $^{30}\text{P} + p$ system, a is the interaction radius [$= 1.25 \times (1^{1/3} + 30^{1/3})$ fm], P_l is the penetrability of the Coulomb and centrifugal barrier for transferred orbital angular momentum l , C is an isospin Clebsch-Gordan coefficient, S is a single-particle spectroscopic factor, and $\theta_{\text{sp},l}^2$ is the dimensionless single-particle reduced width. Note that the spin-parity of a resonance will enter in the rate calculation explicitly [through J_R in Eq. (2)] and implicitly [via P_l , $C^2 S_l$, and $\theta_{\text{sp},l}^2$ in Eq. (3)].

Spin-parity values have been determined experimentally for only six of the 13 known states in ^{31}S within 600 keV of the proton threshold. Moreover, a measurement with superior energy resolution ΔE may help to identify additional states or confirm unambiguously the existence of states only suggested in previous studies (e.g., Refs. [11, 14–16] with $\Delta E \approx 25$ –80 keV). To address these issues and improve calculations of the thermonuclear $^{30}\text{P}(p,\gamma)^{31}\text{S}$ rate in nova explosions, we performed a high-resolution study of the $^{31}\text{P}(^3\text{He},t)^{31}\text{S}$ reaction, measuring ^{31}S excitation energies and

angular distributions. Using our results, we then calculated a new $^{30}\text{P}(p,\gamma)$ rate and performed new hydrodynamic nova simulations to assess the need for additional measurements of J^π values for proton-threshold states in ^{31}S .

II. EXPERIMENT

The $^{31}\text{P}(^3\text{He},t)^{31}\text{S}$ reaction was measured at the Maier-Leibnitz-Laboratorium (MLL) in Garching, Germany over a total period of 6 days. A 25-MeV beam of $^3\text{He}^{2+}$ ions at $I = 500$ –600 nA was delivered by the electron cyclotron resonance (ECR)-like ion source [18] and the MP tandem accelerator to the target position of a quadrupole-dipole-dipole-dipole (Q3D) magnetic spectrograph [19]. Phosphorous targets were prepared at the Technische Universität München using the evaporation method discussed in Ref. [20]: a $26 \mu\text{g}/\text{cm}^2$ layer of ^{31}P was deposited onto a natural carbon foil ($10 \mu\text{g}/\text{cm}^2$) that had been floated onto an aluminum frame. We also used self-supporting natural carbon ($18 \mu\text{g}/\text{cm}^2$) and aluminum ($25 \mu\text{g}/\text{cm}^2$) foil targets to characterize any background and calibrate the focal plane of the spectrograph, respectively. The rectangular entrance aperture to the spectrograph was opened to either 7.0 or 14.3 msr and the beam current was integrated using a Faraday cup at 0° . Light reaction products were momentum analyzed by the Q3D spectrograph and focused onto a multiwire, gas-filled proportional counter backed by a scintillator [21]. Two-dimensional histograms combining two of particle position, energy loss, and residual energy in the focal-plane detector were then produced. Tritons were clearly identified through the sorting of this data offline through software gates, and triton spectra of focal-plane position were then plotted. The $^{31}\text{P}(^3\text{He},t)$ reaction was measured at spectrograph angles of 10.0° , 12.4° , 14.9° , 17.5° , 22.9° , 25.0° , 29.0° , 31.8° , 40.0° , and 55.1° (corresponding to angles over which distinct angular distributions were expected according to preliminary calculations). At any one angle, states in ^{31}S between $E_x \sim 6.1$ –7.1 MeV were observed. Tritons from the $^{12}\text{C}(^3\text{He},t)$ and $^{16}\text{O}(^3\text{He},t)$ reactions were excluded from the detector by virtue of their Q values, and through kinematic analysis it was determined that background due to $(^3\text{He},t)$ reactions on other possible target contaminants was negligible.

III. DATA AND ANALYSIS

Figure 1 shows triton spectra at spectrograph angles of 10° and 17.5° , for the narrow aperture setting (7.0 msr). These spectra were analyzed using least-squares fits of multiple Gaussian or exponentially modified Gaussian functions with a constant background. Consistent excitation energies were determined using each of these prescriptions. Peak widths were fixed to ≈ 12 keV full width at half maximum (FWHM) based on fits of isolated peaks in these spectra.

The focal plane was calibrated at each measurement angle using well-resolved, known states in ^{27}Si populated by the $^{27}\text{Al}(^3\text{He},t)$ reaction, with $6.6 < E_x(^{27}\text{Si}) < 7.6$ MeV. For most of these states in ^{27}Si , $\Delta E_x \approx 3$ keV [22]; for the three highest-energy states (at $E_x(^{27}\text{Si}) = 7469$, 7531, and

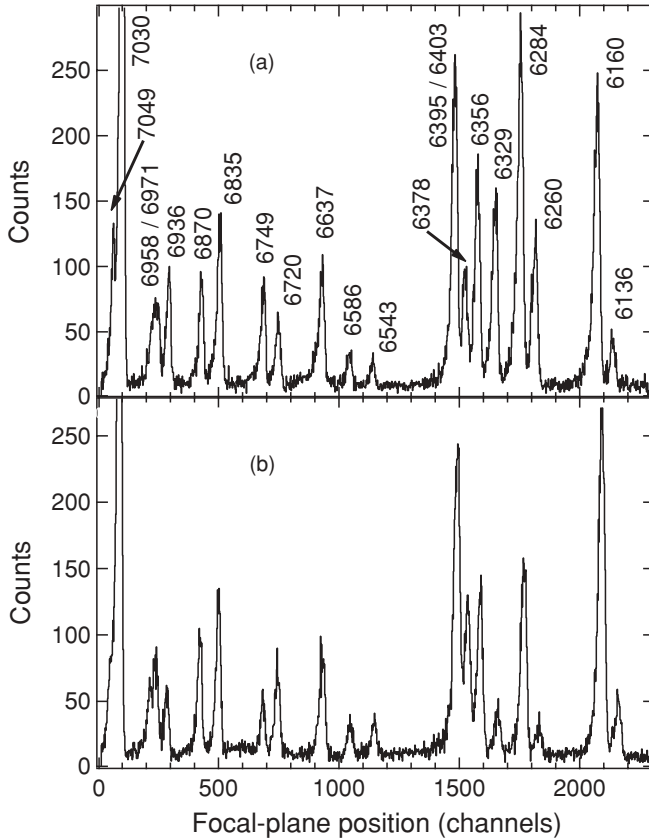


FIG. 1. Focal-plane triton spectra from the $^{31}\text{P}(^3\text{He},t)^{31}\text{S}$ reaction at 25 MeV, $d\Omega = 7.0$ msr, and (a) $\theta_{\text{lab}} = 10^\circ$, (b) $\theta_{\text{lab}} = 17.5^\circ$. Excitation energies are labeled in keV. These spectra have been adjusted relative to one another in channel number to align common states.

7590 keV), $\Delta E_x \approx 0.7$ keV [23]. Second-degree polynomial least-squares fits of triton radius-of-curvature ρ to focal-plane position were obtained at each angle using this information, and these fits were then used to determine excitation energies for states in ^{31}S populated via the $^{31}\text{P}(^3\text{He},t)$ reaction. Table I lists excitation energies from the present work, along with uncertainties due to counting statistics and reproducibility among angles. Each energy from the present work is averaged over at least three angles—the exact number of angles depended upon the magnetic-field setting of the spectrograph during a measurement at a particular angle, the requirement that a ^{31}S state lie within a region spanned wholly by ^{27}Si calibration peaks, and the ability to cleanly resolve a ^{31}S state at a particular angle. In addition, we note a systematic uncertainty of ± 3 keV due to uncertainty in the beam energy ($\Delta E_{\text{beam}} \approx 1$ part in 10 000), and uncertainty in the relative Al and P target thicknesses (each target thickness is known to $\sim 10\%$). Uncertainty in the relative Q value of the $^{27}\text{Al}(^3\text{He},t)$ and $^{31}\text{P}(^3\text{He},t)$ reactions is not significant here largely due to a new measurement of the ^{31}S mass [8] (the relevant masses are now known to better than 0.3 keV [8,9]).

Figure 2 shows triton angular distributions populating states in ^{31}S , fit using calculations from the finite-range

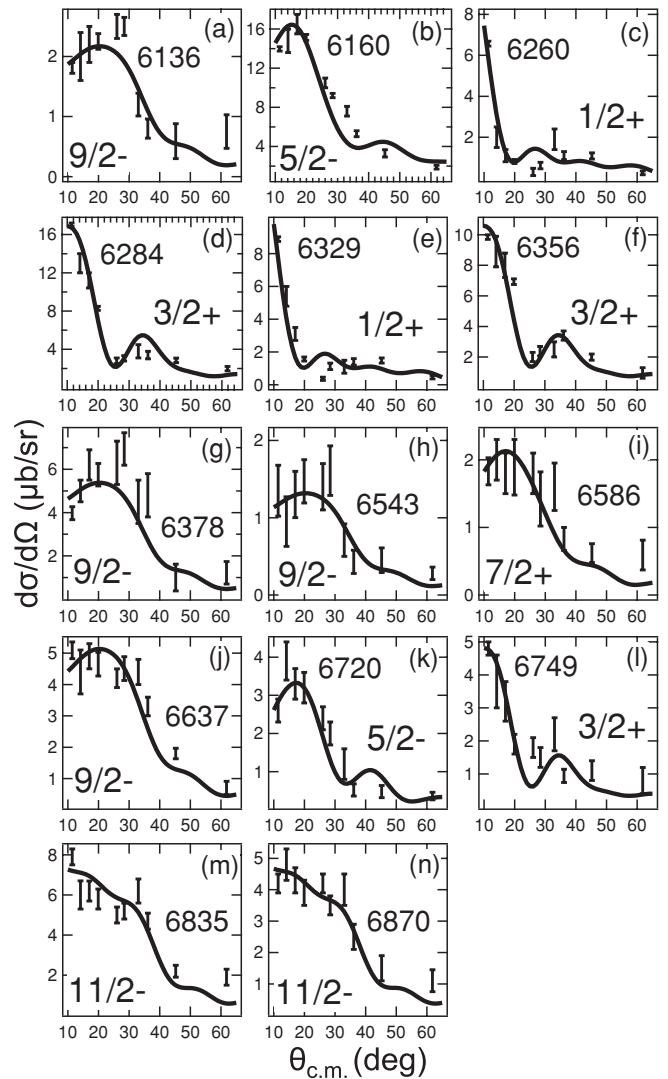


FIG. 2. Triton angular distributions measured with the $^{31}\text{P}(^3\text{He},t)^{31}\text{S}$ reaction at 25 MeV. Curves calculated with the finite-range, coupled-reaction channels code FRESKO [24] have been fit to the data. Each panel (a)–(n) is labeled with the excitation energy (in keV) of the relevant state in ^{31}S and the J^π value of the calculation that best fits the data.

coupled-reaction channels code FRESKO [24]. An angular distribution analysis was only attempted for states clearly observed over at least five angles. The $(^3\text{He},t)$ charge-exchange reaction has been treated as a two-step (sequential) single-nucleon transfer reaction via the intermediate $^{32}\text{S} + d$ channel (which dominates over the intermediate $^{30}\text{P} + \alpha$ channel). The shapes of the angular distributions calculated in this manner are similar to those from the one-step process [25,26]. The optical model parameters for the calculation were taken from Ref. [27] for the $^3\text{He} + \text{nucleus}$ potential, and from Ref. [28] for the deuteron, where the $(^3\text{He},d)$ reaction had been studied at the same beam energy of 25 MeV. The triton optical model parameters were calculated using global parameter scaling formulas [29]. The depth of the proton and neutron binding potentials were adjusted to reproduce the respective separation energies. Tests with a modified

TABLE I. Nuclear structure of ^{31}S above the $^{30}\text{P} + p$ threshold [$S_p = 6130.9(4)$ keV [8,9]]. Excitation energies are given in keV with uncertainties due to statistics and reproducibility. In addition, a ± 3 keV uncertainty arises from systematic uncertainties (see text); the good agreement between energies from the present work and those from past work indicate that the systematic uncertainty may be overestimated. Only J^π values based upon experimental data are listed and adopted here (e.g., values based upon tentative mirror assignments from past studies are not included).

Endt [22]	$(^3\text{He},\alpha)$ [11]	$(\beta^+ \nu)$ [12]	$(^{20}\text{Ne}, n\gamma)$ [13]	(p,d) [14]	$(^3\text{He},t)$ [15,16]	$(^3\text{He},t)$ Present	Adopted
					6134(2)	6136(1)	6135.6(9)
						9/2	9/2
6155(10)			6160.2(7)		6160(3)	6160(1)	6160.1(6)
			5/2 ⁻			5/2	5/2-
6267(10)	6257(5)			6267(5)	6259(2)	6260(1)	6260.0(9)
1/2 ⁺	1/2 ⁺			1/2 ⁺		1/2 ⁺	1/2 ⁺
6268(10)		6280(2)			6283(2)	6284(1)	6283.2(8)
3/2 ⁺		3/2 ⁺				3/2 ⁺	3/2 ⁺
					6327(2)	6329(1)	6328.6(9)
						1/2 ⁺	1/2 ⁺
6350(11)					6357(2)	6356(1)	6356.1(9)
						3/2 ⁺	3/2 ⁺
			6376.9(5)		a	6378(1)	6377.1(4)
			9/2 ⁻			9/2	9/2 ⁻
	6393(5)		6393.7(5)		a	6395(2)	6393.8(5)
			11/2 ⁺				11/2 ⁺
6396(10)				6411(9)	6401(3)	6403(2)	6402.2(16)
6543(11)				6546(15)	6543(2)	6543(1)	6543.0(9)
						(7/2, 9/2)	(7/2, 9/2)
[6593(15)]					6585(2)	6586(1)	6585.8(9)
						7/2	7/2
6628(13)			6636.3(15)		6639(3)	6637(1)	6636.9(8)
			9/2 ⁻			9/2	9/2 ⁻
6712(11)					6720(2)	6720(1)	6719.9(9)
					(1/2 ⁺ - 9/2 ⁻)	5/2	5/2
6748(10)					6749(2)	6749(1)	6749.0(9)
					(7/2 ⁻ , 9/2 ⁻)	3/2 ⁺	3/2 ⁺
6796(25)							6796(25)
6835(9)			6833.4(3)	6848(9)	6836(2) ^b	6835(1)	6833.6(3)
			11/2 ⁻		(1/2 ⁺ - 9/2 ⁻)	11/2	11/2 ⁻
6870(10)					6872(2)	6870(1)	6870.4(9)
					$\geq 1/2^-$	11/2	11/2
6921(25)		6921(15)			6939(3)	6936(2)	6936.7(17)
		(1/2 - 5/2) ⁺					(1/2 - 5/2) ⁺
6996(15)	6966(5)				6961(3)	6958(2)	6959.6(16)
	1/2 ⁺				(1/2 ⁺ - 9/2 ⁻)		1/2 ⁺
					[6975(3)]	6971(2)	6972.2(17)
7039(10)	7033(5)	7012(16)		7044(6)	7036(2) ^b	7030(2)	7033.5(13)
(3/2, 5/2) ⁺	(3/2, 5/2) ⁺	(1/2, 3/2, 5/2) ⁺		5/2 ⁺			(1/2, 3/2, 5/2) ⁺
					[7053(2)]	7049(2)	7051.0(14)

^aObserved but energy not measured.

^bListed as a doublet.

triton potential showed that the influence of this parameter on the shapes of the angular distributions is not significant. The first step of the reaction was fixed to the experimental single-nucleon transfer data of Ref. [28]. In addition to the states which were strongly populated in the $(^3\text{He},d)$ reaction, negative-parity states in ^{32}S were also included in the coupling scheme.

The assignment of spin and parity to the final states in ^{31}S is based primarily upon how fast the $^{31}\text{P}(^3\text{He},t)$ cross

section drops with increasing scattering angle. The identification of $1/2^+$ and $3/2^+$ states is straightforward due to the characteristic shapes of these angular distributions. The large number of possible couplings makes it difficult to distinguish between positive and negative parity for higher spins. Given these considerations, we suppress the parity designations in Table I for ^{31}S states with $J > 3/2$ (although in Fig. 2 the specific curves that gave the best fits to the measured angular distributions are included for completeness).

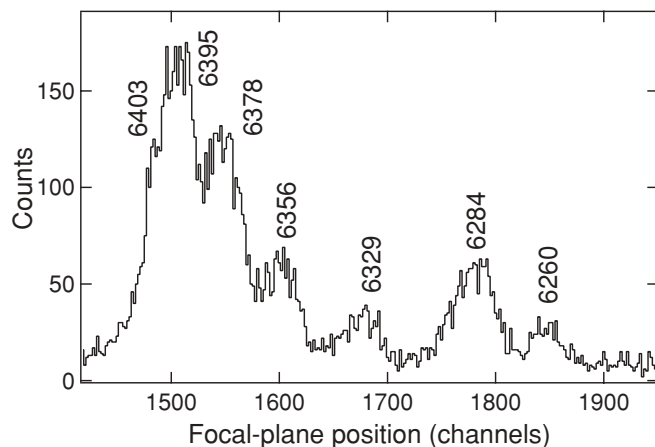


FIG. 3. Partial focal-plane triton spectrum from the $^{31}\text{P}(^3\text{He},t)^{31}\text{S}$ reaction at 25 MeV, $d\Omega = 14.3$ msr, and $\theta_{\text{lab}} = 25^\circ$. Excitation energies are labeled in keV. The 6403 keV state suggested from a previous lower-resolution study of this reaction [15] is evident.

IV. DISCUSSION

Results from the present work are compared, in Table I, with recent studies of the structure of ^{31}S above the proton threshold. Overall, the ^{31}S excitation energies extracted from the present study are in good agreement with previous studies, in particular, with a recent study of this same reaction [15,16]. The impact of the superior energy resolution of the Q3D spectrograph is apparent, e.g., from a comparison between our Fig. 1 ($\Delta E \approx 12$ keV) and Fig. 1 in Ref. [15] ($\Delta E \approx 25$ keV). We clearly observe states at 6403 keV (see Fig. 3), 6936, 6958, 6971, 7030, and 7049 keV which had not been resolved previously (but had been identified through analysis [15,16]). We find no evidence for a doublet at 6835 keV nor at 7030 keV, and, as all recent studies, we do not observe a state at 6796 keV. For the state at 6835 keV, a doublet was assumed in Ref. [16] to reconcile the detection of a proton branch from a state at this energy [populated through $^{31}\text{P}(^3\text{He},t)$], as well as the presence of a known high-spin state ($J^\pi = 11/2^-$) at 6833.4(3) keV [13]. We find that the state we observe is consistent with $J = 11/2$ character, and consequently, we remove the designation of a doublet at this energy in Table I. It is somewhat difficult to identify the two states we observe for $E_x > 7$ MeV with corresponding states (and J^π constraints) from previous studies. It seems clear that there are two or three levels between 7.00 and 7.05 MeV; in the “adopted” column of Table I, we have chosen to list two levels in this energy region.

The J^π values we find from our angular distributions are also in good agreement with previous experimental determinations (see Table I). However, the assignment of mirror states between the nuclei ^{31}S and ^{31}P [16] is further complicated because of our new J^π constraints, and new states in ^{31}P seem necessary for a cogent scheme. Experimental constraints on J^π values are now available for all ^{31}S states within 600 keV of the $^{30}\text{P} + p$ threshold except the 6403 keV state.

We use this new information to calculate a thermonuclear $^{30}\text{P}(p,\gamma)^{31}\text{S}$ rate applicable over temperatures encountered in ONe nova explosions. Given that no measurements exist for (p,γ) resonance strengths or partial widths for any ^{31}S states below 6.7 MeV, our main intent here is to examine the effect of the remaining uncertainties in the J^π values of these states. We consider 16 states in ^{31}S between the proton threshold and 6.9 MeV for these calculations (not including the 6796 keV state). Resonance energies were calculated using the adopted excitation energies of Table I and the $^{30}\text{P}(p,\gamma)^{31}\text{S}$ Q value of 6130.9(4) keV [8,9]. For the four highest-energy states at 6720, 6749, 6834, and 6870 keV, we use the measured proton branching ratios of Ref. [16]. We determine a “low” rate assuming the 6402, 6543, and 6586 keV states have $J^\pi = \{7/2^+, 9/2^+, 7/2^-\}$ (and therefore $l_{\text{min}} = \{2, 4, 3\}$) and a “high” rate assuming these three states have $J^\pi = \{5/2^-, 7/2^+, 7/2^+\}$ (and therefore $l_{\text{min}} = \{1, 2, 2\}$). Note that the above J^π assignments for the 6402 keV state are somewhat arbitrary since no experimental information is available for the J^π of this state (see Table I). For this sensitivity test, however, we simply rely on constraints from possible ^{31}P mirror levels for this state (but see below). The 6136 keV state is assumed to be $9/2^-$, though its contribution to the total rate is negligible at nova temperatures. We treat the $J^\pi = 1/2^+$, 6260 keV state in the same manner as Ref. [13], where both $l = 0$ and $l = 2$ contributions are considered (along with shell model calculations for the associated spectroscopic factors).

To demonstrate the uncertainty inherent to calculations of the $^{30}\text{P}(p,\gamma)^{31}\text{S}$ rate, we use a Monte Carlo treatment following the prescription of Ref. [2]. This is useful in particular to account for the unknown proton spectroscopic factors [see Eq. (3)] and γ -ray partial widths involved (as well as the uncertainties in the four measured proton branching ratios of Ref. [16], and in all resonance energies). To calculate the proton partial widths, we use Eq. (3) with Porter-Thomas probability density distributions for the dimensionless reduced widths $\theta_p^2 = C^2 S \theta_{\text{sp}}^2$. The mean value of θ_p^2 was set to 0.0045 as this seems to best describe experimental dimensionless reduced widths determined for unbound states over the $A =$

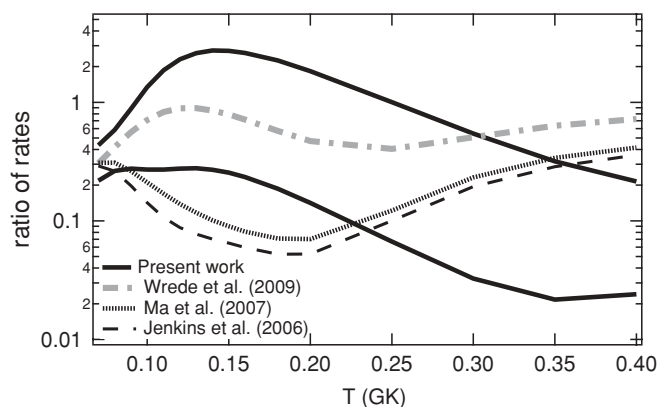


FIG. 4. Ratios of the “high” (upper solid line) and “low” (lower solid line) $^{30}\text{P}(p,\gamma)^{31}\text{S}$ reaction rates from the present work (see text) and the rates of Wrede *et al.* (2009) [16], Ma *et al.* (2007) [14], and Jenkins *et al.* (2006) [13] to the statistical-model rate [31] used in the nova models of Jose *et al.* (2001) [6].

24–40 mass range (see Fig. 4 of Ref. [2]). The upper limits for these distributions were found individually for each state using $C^2S = 1$ along with calculations from Ref. [30] for the dimensionless single-particle reduced widths θ_{sp}^2 . For the unknown γ -ray partial widths, a reasonable statistical treatment is currently unavailable. The uncertainty distribution of γ -ray partial widths is, however, less critical for calculating reaction rates using unbound states just above the proton threshold [2]. We have used log-normal probability distributions with mean values of $\Gamma_\gamma = 0.15$ eV [13] and standard deviations corresponding to 50% of this mean value.

Figure 4 shows our high and low $^{30}\text{P}(p,\gamma)^{31}\text{S}$ thermonuclear rates normalized to the statistical-model rate [31] used in the nova models of José *et al.* (2001) [6]. Several details should be noted given that a Monte Carlo treatment has been used to calculate these rates. For a given temperature, the median low (high) rate would correspond to the 0.50 quantile of the cumulative distribution of low (high) rates. In Fig. 4, though, for each temperature we have chosen to show the 0.16 quantile of the low rates and the 0.84 quantile of the high rates. (We also use these rates for the nova calculations discussed below, and will refer to them as the “low” and “high” rates, respectively.) The distributions of low rates and high rates intersect substantially as a function of temperature because of the unknown proton spectroscopic factors. Over 0.1–0.4 GK, the ratio between the 0.16 quantile of the high rates and the 0.16 quantile of the low rates is ≈ 3 ; the ratio between the 0.84 quantile of the high rates and the 0.84 quantile of the low rates is ≈ 2 . For example, at $T = 0.25$ GK, the 0.16 quantile of the low rates is $4.6 \times 10^{-5} \text{ cm}^3 \text{ s}^{-1} \text{ mol}^{-1}$, the median low rate is $1.6 \times 10^{-4} \text{ cm}^3 \text{ s}^{-1} \text{ mol}^{-1}$, and the 0.84 quantile of the low rates is at $4.8 \times 10^{-4} \text{ cm}^3 \text{ s}^{-1} \text{ mol}^{-1}$. The 0.16 quantile of the high rates at 0.25 GK is at $1.0 \times 10^{-4} \text{ cm}^3 \text{ s}^{-1} \text{ mol}^{-1}$, the median high rate is $2.9 \times 10^{-4} \text{ cm}^3 \text{ s}^{-1} \text{ mol}^{-1}$, and the 0.84 quantile of the high rates is at $6.9 \times 10^{-4} \text{ cm}^3 \text{ s}^{-1} \text{ mol}^{-1}$. For more details, see Ref. [2].

Also shown in Fig. 4 are the rates of Wrede *et al.* (2009) [16], Ma *et al.* (2007) [14], and Jenkins *et al.* (2006) [13] normalized to the rate used in Ref. [6]. Note that if we assume the direct proton capture S factor at zero bombarding energy as $S_{\text{DC}}(0) = 91.2$ keV b (from an average of measured $S_{\text{DC}}(0)$ values around ^{30}P [1]), the direct-capture component of this rate is negligible below 0.04 GK. The rates of Refs. [13] and [14] did not include the contribution of states in ^{31}S that were subsequently observed by Wrede *et al.* [15,16] and in the present work. The rate from Ref. [16] is within a factor of ≈ 2 of the statistical-model rate for the temperatures shown in Fig. 4. Note an error in Fig. 9 of Ref. [16]: above ≈ 2 GK, the comparison made in that plot between different $^{30}\text{P}(p,\gamma)^{31}\text{S}$ rates is not completely valid as a stellar enhancement factor (SEF) was included for the statistical model rate but not the other rates shown in that plot. This is not a problem here (e.g., for our Fig. 4) as we are only interested in the $^{30}\text{P}(p,\gamma)$ rate (and consequences of this rate) at temperatures below ≈ 0.4 GK (over which the $\text{SEF} = 1$ [32]). We do remark, however, that the statistical model rate is stated to be most accurate only for temperatures not significantly below ≈ 0.24 GK [32].

First, and perhaps most relevant to the present study, is the large spread between our high and low $^{30}\text{P}(p,\gamma)$ rates; this

can be attributed directly to the uncertainties in the exact J^π values of the 6402, 6543, and 6586 keV states in ^{31}S and to the unknown proton spectroscopic factors (as discussed above). Between $T = 0.07$ and 0.4 GK, the ratio between the high and low rates varies between a factor of 2 and a factor of 20 (the latter at $T = 0.3$ GK). The dominant contributions to the high rate are from the $l = 0$ component of the 129 keV resonance ($E_x = 6260$ keV) between 0.03 and 0.08 GK, the 196 and 225 keV ($l = 0$, $E_x = 6329$ keV; $l = 0$, $E_x = 6356$ keV) resonances from 0.08 to 0.15 GK, the 225 keV resonance from 0.15 to 0.3 GK, and the 271 keV (assumed $l = 1$, $E_x = 6402$ keV) resonance from 0.3 GK to 0.5 GK. For the low rate, the dominant contributions are similar at low temperatures with the $l = 0$ component of the 129 keV resonance dominating below 0.08 GK, and the 196 and 225 keV resonances contributing roughly equally between 0.08 and 0.15 GK. In this case, though, the 225 keV ($l = 0$) resonance alone dominates the rate between 0.15 and 0.5 GK (recall that the 271 keV resonance is assigned with $l = 2$ for the low rate calculations). The clear influence of the (unknown) J^π value of the 6402 keV state on the overall $^{30}\text{P}(p,\gamma)$ rate is evident here from the above comparison of the role it plays in the high and low rates. For example, if we had assumed this state as $l = 0$ (rather than $l = 1$) for the high rate calculation, it would become a still more dominant contributor around the highest temperatures achieved in ONe nova explosions ($T = 0.3$ –0.4 GK), increasing the overall rate further.

Since our high and low rates arise from a Monte Carlo treatment and the rate from Ref. [16] does not, it is difficult to compare these rates directly. To facilitate this, we have recalculated the rate of Wrede *et al.* [16] using the same assumptions for l transfer in that study (which are, in general, different from the values we use for our high and low rates), but now with the Monte Carlo treatment discussed above for the unknown spectroscopic factors and γ -ray partial widths. To illustrate the effects, we examine two particular temperatures. At $T = 0.15$ GK, our low (high) rate is factor of 3.1 lower (3.4 higher) than the published Wrede *et al.* rate. But the recalculated Wrede *et al.* rate is a factor of 5.3 lower than the published Wrede *et al.* rate at this temperature. Therefore, the different assumptions in J^π values for our rates and the Wrede *et al.* rate account for a factor of $5.3/3.1 = 1.7$ enhancement (comparing our low rate to the recalculated Wrede *et al.* rate) and a factor of $3.4 \times 5.3 = 18$ enhancement (comparing our high rate to the recalculated Wrede *et al.* rate). At $T = 0.35$ GK, the recalculated Wrede *et al.* rate is a factor of 4.0 lower than the published Wrede *et al.* rate. With similar considerations as above, the different assumptions in J^π values for our rates and the Wrede *et al.* rate account for a factor of 7.3 reduction (comparing our low rate to the recalculated Wrede *et al.* rate) and a factor of 2.0 enhancement (comparing our high rate to the recalculated Wrede *et al.* rate).

Given the large differences between our new rates and the rate used in the nova models of José *et al.* (2001) [6], we have performed a new set of hydrodynamic nova simulations to explore the corresponding impact on nucleosynthesis in classical nova explosions. We have used SHIVA, a one-dimensional (spherically symmetric), hydrodynamic, implicit, Lagrangian code used extensively in the modeling of novae

TABLE II. Mean composition of nova ejecta (in mass fractions, for Si-Ca isotopes) from models of nova explosions on $1.35M_{\odot}$ ONe white dwarfs. The only difference between models A, B and C is the $^{30}\text{P}(p,\gamma)^{31}\text{S}$ rate used (the “low” and “high” rates are from the present work, see text and Fig. 4).

Isotope	Model		
	A (SMOKER [31])	B (low)	C (high)
^{30}Si	1.15×10^{-2}	5.71×10^{-2}	1.40×10^{-2}
^{31}P	9.16×10^{-3}	4.68×10^{-3}	9.69×10^{-3}
^{32}S	5.56×10^{-2}	1.97×10^{-2}	5.30×10^{-2}
^{33}S	8.53×10^{-4}	2.52×10^{-4}	7.92×10^{-4}
^{34}S	3.87×10^{-4}	1.12×10^{-4}	3.57×10^{-4}
^{35}Cl	4.11×10^{-4}	1.20×10^{-4}	3.78×10^{-4}
^{36}Ar	5.49×10^{-5}	1.71×10^{-5}	5.05×10^{-5}
^{37}Cl	1.51×10^{-4}	6.90×10^{-5}	1.42×10^{-4}
^{38}Ar	2.46×10^{-5}	1.90×10^{-5}	2.40×10^{-5}
^{39}K	5.95×10^{-6}	6.08×10^{-6}	5.96×10^{-6}
^{40}Ca	3.06×10^{-5}	3.06×10^{-5}	3.06×10^{-5}
^{41}K	1.97×10^{-9}	2.17×10^{-9}	1.99×10^{-9}

[33] and type I x-ray bursts [34], and have computed three different models of nova outbursts, with identical input physics except for the specific choice of the $^{30}\text{P}(p,\gamma)^{31}\text{S}$ rate adopted. Model A uses the SMOKER rate [31], as in the models of Ref. [6], and models B and C use the low and high rates from the present work (Fig. 4), respectively. In all three cases, we have assumed accretion of solar-like matter (preenriched with 50% of white dwarf core material to mimic the mixing processes acting at the core-envelope interface [6]) at a rate of $\dot{M}_{\text{acc}} = 2 \times 10^{-10} M_{\odot} \text{ yr}^{-1}$ onto a $1.35M_{\odot}$ ONe white dwarf. As expected, whereas no differences are found in the dynamics of the explosion for the three models computed [since the $^{30}\text{P}(p,\gamma)^{31}\text{S}$ reaction is not a major contributor to the energy production], significant differences in the mean chemical composition of the ejected envelope are found. As shown in Table II, the main differences between models B and C are restricted to the Si-Ar mass region. (models A and C give similar results.) The ratio between the mean $^{32,33,34}\text{S}$, ^{35}Cl , and ^{36}Ar yields obtained in models C and B is ≈ 3 while the change in ^{31}P and ^{37}Cl is somewhat lower (ratios ≈ 2). Note also the large reduction (by a factor of 4) in the final ^{30}Si yield due to the high $^{30}\text{P}(p,\gamma)$ rate of model C. Resolving these differences between model predictions is clearly important for the quantitative comparison of nova yields, inferred theoretically and observationally, in the Si-Ar mass region. As well, presolar nova grains likely condensed in the ejecta from massive ONe white dwarfs are usually identified by large $^{30}\text{Si}/^{28}\text{Si}$ excesses with respect to the solar ratio [7]. Whereas a low $^{30}\text{P} + p$ rate favors the β^+ decay of ^{30}P into ^{30}Si , a larger rate will efficiently destroy ^{30}P and would imply a dramatic decrease in the final ^{30}Si content (e.g., the results of model C), hence questioning the nova paternity of these meteoritic grains. It is therefore crucial to reduce the uncertainty associated with the rate of the $^{30}\text{P}(p,\gamma)^{31}\text{S}$ reaction.

V. CONCLUSIONS

Through a high-resolution study of the $^{31}\text{P}(^3\text{He},t)^{31}\text{S}$ reaction over $E_x(^{31}\text{S}) = 6.1\text{--}7.1$ MeV, we have confirmed previous states and have clearly observed six states that had been discovered (some only tentatively) previously using lower-resolution data. For the first time we have measured $^{31}\text{P}(^3\text{He},t)$ angular distributions for proton-threshold states in ^{31}S ; calculations using a sequential transfer mechanism via the $^{32}\text{S} + d$ channel yield reasonable fits to the data. With this information, experimental J^{π} assignments or constraints are now available for all ^{31}S states between the proton threshold and $E_x = 6.7$ MeV except one (the 6402 keV state). Given the lack of experimental resonance strength (or partial width) measurements for these low-energy states, this is critical information needed to determine the key $^{30}\text{P}(p,\gamma)^{31}\text{S}$ rate in classical nova explosions.

We have also explored the astrophysical impact of remaining uncertainties in the J^{π} values of the 6402, 6543, and 6586 keV states in ^{31}S and the unknown proton spectroscopic factors. The $^{30}\text{P}(p,\gamma)^{31}\text{S}$ rate may vary by as much as a factor of 20 over typical nova peak temperatures due to these uncertainties. In turn, our simulations of novae on massive ONe white dwarfs demonstrate that these uncertainties may affect nova yields of Si-Ar isotopes by as much as a factor of 4. One must be careful with the interpretation of these results given the total lack of experimental partial widths and/or proton spectroscopic factors for states most relevant to the calculation of this rate over nova temperatures. Nonetheless, until direct measurements are possible, it is important to identify and minimize all uncertainties involved in current calculations of this rate as much as possible. Additional measurements are therefore required to determine these J^{π} values exactly (and confirm the other assignments from the present and previous studies). Indeed, such experiments are already underway [35] and we reserve the tabulation of a new $^{30}\text{P}(p,\gamma)^{31}\text{S}$ rate until these results are available. Finally, we stress the need to develop high-intensity radioactive beams of ^{30}P ($>10^6$ ions s^{-1} [36]) to measure the $^{30}\text{P}(p,\gamma)^{31}\text{S}$ reaction directly at astrophysical energies relevant to nova explosions.

ACKNOWLEDGMENTS

It is a pleasure to thank the crew of the MLL tandem accelerator. We also thank T. Rauscher for noting the error in Fig. 9 of Ref. [16]. This work was supported by the DFG cluster of excellence “Origin and Structure of the Universe” (www.universe-cluster.de). A.P., J.J., and R.L. were partially supported by the Spanish MICINN Grants No. AYA2010-15685 and No. EUI2009-04167, by the E.U. FEDER funds, and by the ESF EUROCORES Program EuroGENESIS. A.A.C. was supported, in part, by a Grant from NSERC Canada. J.A.C. and C.M.D. acknowledge support from the US Department of Energy, Office of Nuclear Physics, under Contract No. DE-AC02-06CH11357. C.M.D. was also partially supported by JINA Grant No. PHY0822648. C.W. acknowledges support from the US Department of Energy under Contract No. DE-FG02-97ER41020.

- [1] C. Iliadis, J. M. D'Auria, S. Starrfield, W. J. Thompson, and M. Wiescher, *Astrophys. J. Suppl.* **134**, 151 (2001).
- [2] R. Longland, C. Iliadis, A. E. Champagne, J. R. Newton, C. Ugalde, A. Coc, and R. Fitzgerald, *Nucl. Phys. A* **841**, 1 (2010).
- [3] J. José and M. Hernanz, *J. Phys. G* **34**, R431 (2007).
- [4] J. José, J. Casanova, F. Moreno, E. García-Berro, A. Parikh, and C. Iliadis, in *Proceedings of Tours Symposium on Nuclear Physics and Astrophysics VII*, AIP Conf. Proc. No. 1238 (AIP, Melville, NY, 2010), p. 157.
- [5] C. Iliadis, A. Champagne, J. José, S. Starrfield, and P. Tupper, *Astrophys. J. Suppl.* **142**, 105 (2002).
- [6] J. José, A. Coc, and M. Hernanz, *Astrophys. J.* **560**, 897 (2001).
- [7] J. José, M. Hernanz, S. Amari, K. Lodders, and E. Zinner, *Astrophys. J.* **612**, 414 (2004).
- [8] A. Kankainen *et al.*, *Phys. Rev. C* **82**, 052501(R) (2010).
- [9] G. Audi, A. H. Wapstra, and C. Thibault, *Nucl. Phys. A* **729**, 337 (2003).
- [10] C. Iliadis, *Nuclear Physics of Stars* (Wiley-VCH, Weinheim, 2007).
- [11] J. Vernotte, G. Berrier-Ronsin, S. Fortier, E. Hourani, A. Khendriche, J. M. Maison, L.-H. Rosier, G. Rotbard, E. Caurier, and F. Nowacki, *Nucl. Phys. A* **655**, 415 (1999).
- [12] A. Kankainen *et al.*, *Eur. Phys. J. A* **27**, 67 (2006).
- [13] D. G. Jenkins *et al.*, *Phys. Rev. C* **73**, 065802 (2006).
- [14] Z. Ma *et al.*, *Phys. Rev. C* **76**, 015803 (2007).
- [15] C. Wrede, J. A. Caggiano, J. A. Clark, C. Deibel, A. Parikh, and P. D. Parker, *Phys. Rev. C* **76**, 052802(R) (2007).
- [16] C. Wrede, J. A. Caggiano, J. A. Clark, C. M. Deibel, A. Parikh, and P. D. Parker, *Phys. Rev. C* **79**, 045803 (2009).
- [17] L. Trache *et al.*, in *Proceedings of Tenth Symposium on Nuclei in the Cosmos*, PoS (NIC-X) 163 (2008).
- [18] R. Hertzenberger, A. Metz, Y. Eisermann, K. El Abiary, A. Ludewig, C. Pertl, S. Treib, H.-F. Wirth, P. Schiemenz, and G. Graw, *Nucl. Instrum. Methods Phys. Res. A* **536**, 266 (2005).
- [19] M. Löffler, H. J. Scheerer, and H. Vonach, *Nucl. Instrum. Methods* **111**, 1 (1973).
- [20] H.-S. Tzeng, J.-Y. Liu, I. Sugai, and Y. C. Liu, *Nucl. Instrum. Methods* **150**, 143 (1978).
- [21] H.-F. Wirth, H. Angerer, T. von Egidy, Y. Eisermann, G. Graw, and R. Hertzenberger, Maier-Leibnitz-Laboratorium Annual Report, p. 71 (unpublished).
- [22] P. M. Endt, *Nucl. Phys. A* **521**, 1 (1990); **633**, 1 (1998).
- [23] G. Lotay, P. J. Woods, D. Seweryniak, M. P. Carpenter, R. V. F. Janssens, and S. Zhu, *Phys. Rev. Lett.* **102**, 162502 (2009).
- [24] I. J. Thompson, *Comput. Phys. Rep.* **7**, 167 (1988); [<http://www.fresco.org.uk>].
- [25] C. N. Pinder *et al.*, *Nucl. Phys. A* **533**, 25 (1991).
- [26] C. Gaarde, J. S. Larsen, M. N. Harakeh, S. Y. van der Werf, M. Igarashi, and A. Müller-Arnke, *Nucl. Phys. A* **334**, 248 (1980).
- [27] J. Vernotte, G. Berrier-Ronsin, J. Kalifa, and R. Tamisier, *Nucl. Phys. A* **390**, 285 (1982).
- [28] J. Vernotte, G. Berrier-Ronsin, J. Kalifa, R. Tamisier, and B.H. Wildenthal, *Nucl. Phys. A* **571**, 1 (1994).
- [29] C. M. Perey and F. G. Perey, *At. Data Nucl. Data Tables* **17**, 1 (1976).
- [30] C. Iliadis, *Nucl. Phys. A* **618**, 166 (1997).
- [31] F.-K. Thielemann, M. Arnould, and J. W. Truran, in *Advances in Nuclear Astrophysics*, edited by E. Vangioni-Flam (Editions Frontière, Gif-sur-Yvette, 1987), p. 525.
- [32] T. Rauscher and F.-K. Thielemann, *At. Data Nucl. Data Tables* **75**, 1 (2000).
- [33] J. José and M. Hernanz, *Astrophys. J.* **494**, 680 (1998).
- [34] J. José, F. Moreno, A. Parikh, and C. Iliadis, *Astrophys. J. Suppl.* **189**, 204 (2010).
- [35] D. Irvine, A. A. Chen *et al.* (private communication).
- [36] D. A. Hutcheon *et al.*, TRIUMF EEC proposal S1108 (unpublished).